

Pamukkale Üniversitesi Mühendislik Bilimleri Dergisi

Pamukkale University Journal of Engineering Sciences



Improvement of water flux, treatment efficiency, and fouling resistance of polyethersulfone/cellulose acetate blend ultrafiltration membranes using nanomaterials derived from renewable resources

Yenilenebilir kaynaklardan elde edilen nanomalzemeler kullanılarak polietersülfon/selüloz asetat karışımı ultrafiltrasyon membranlarının su akısının, arıtma veriminin ve kirlenme direncinin iyileştirilmesi

Seren Acaeer Arat1*

¹Department of Environmental Engineering, İstanbul Technical University, İstanbul, Türkiye, acarerseren@gmail.com

Received/Geliş Tarihi: 30.05.2025 Accepted/Kabul Tarihi: 27.10.2025 Revision/Düzeltme Tarihi: 24.10.2025

doi: 10.65206/pajes.70729 Research Article/Arastırma Makalesi

Abstract

Polymeric flat sheet membranes are extensively applied in both largeand small-scale water and wastewater treatment processes. A straightforward and effective strategy to enhance the performance of polymer-based flat sheet membranes, particularly their water flux and treatment efficiency, is the integration of nanomaterials into the membrane structure. In this research, cellulose nanocrystals (CNC) and cellulose nanofibrils (CNF) were incorporated into polyethersulfone (PES)/cellulose acetate (CA) blend membranes, which were produced using the non-solvent induced phase separation technique. The prepared membranes underwent comprehensive characterization, and their water flux and turbidity removal performance were subsequently evaluated using the classical filtration technique. Morphological properties, including porosity, mean pore size, and pore size distribution, were analyzed from SEM images processed in MATLAB Antifouling behavior (Rt, Rir, Rr, FRR, and FDR) and resistance related (RT, RM, RIR, and RR) parameters were evaluated. Incorporation of CNC and CNF improved the hydrophilicity and porosity of the PES/CA membranes while simultaneously decreasing average pore size and surface roughness. Furthermore, both reinforcements significantly increased the pure water flux of the membranes, with observed increased the pure water flux of the membranes, with observed enhancements of 33.49% for CNC and 37.56% for GNF, reaching a maximum flux of 365.12 L/m²-h. Turbidity removal performance was also positively influenced by the presence of nanomaterials, with the PES/CA/CNF membrane achieving the highest removal efficiency of 98.24%. Overall, CNF was superior to CNC in enhancing the membrane's porosity, hydrophilicity, surface smoothness, water flux, turbidity removal, and fouling resistance. The estimated fabrication cost for PES/CA-based membranes ranged from 1773 to 2948 TRY.

Keywords: membrane, cellulose nanocrystal, cellulose nanofibril, characterization, ultrafiltration, water treatment

Öz

Polimerik düz levha membyanla, hem büyük hem de küçük ölçekli su ve atık su arıtım prose lerinde yaygın olarak kullanılmaktadır. Polimer bazlı düz levha membyanların performansını, özellikle su akısı ve arıtım verimliliğini attırmının basit ve etkili bir yolu, nanomalzemelerin membran yayısını entegre edilmesidir. Bu çalışmada, selüloz membran yayısını entegre edilmesidir. Bu çalışmada, selüloz nanokrista'ler (LNC) ve selüloz nanofibriller (CNF), çözücü olmayan tarafı dan meüklenen faz ayırma yöntemi kullanılarak üretilen polieters ilfon (PES)/selüloz asetat (CA) karışım membranlara dahil edilmiş ir. Hazırlanan membranlar kapsamlı karakterizasyondan geçirilmiş ve su akısı ile bulanıklık giderme performansları klasik filtrasyon tekniği kullanılarak değerlendirilmiştir. Porozite, ortalama gözenek boyutu ve gözenek boyutu dağılımı gibi morfolojik özellikler, MATLAB ile işlenen SEM görüntülerinden analiz edilmiştir. Antifouling davranışı (Rt, Rir, Rr, FRR ve FDR) ve dirençle ilgili parametreler (RT, RM, RIR ve RR) değerlendirilmiştir. CNC ve CNF'nin eklenmesi, PES/CA membranlarının hidrofiliğini ve porozitesini artırırken, ortalama gözenek boyutu ve yüzey pürüzlülüğünü azaltmıştır. Ayrıca, her iki katkı da membranların saf su akısını önemli ölçüde artırmış, CNC için %33,49 ve CNF için %37,56 artış gözlemlenmiş ve maksimum akış 365,12 L/m²·h'ye ulaşmıştır. Bulanıklık giderme performansı da nanomalzemelerin varlığından olumlu etkilenmiş olup, PES/CA/CNF membranı en yüksek giderim verimi olan %98,24'e ulaşmıştır. Genel CNF, membranın porozitesini, hidrofiliğini, yüzey pürüzsüzlüğünü, su akısını, bulanıklık giderimini ve kirlenmeye karşı direncini artırmada CNC'ye kıyasla daha üstün performans göstermiştir. PES/CA bazlı membranların tahmini üretim maliyeti 1773 ile 2948 TRY arasında değişim göstermiştir.

Anahtar kelimeler: membran, selüloz nanokristal, selüloz nanofibril, karakterizasyon, ultrafiltrasyon, su arıtımı

1 Introduction

Ensuring access to clean water for all, controlling water pollution and ensuring sustainable water management are among the global sustainable development goals [1]. Membrane processes are advanced treatment processes that provide higher contaminant removal efficiency, more space-saving and more chemical saving compared to conventional treatment processes [2]. Membrane filtration processes are commonly applied in diverse fields, including drinking water treatment, greywater treatment, municipal wastewater

treatment, seawater treatment, landfill leachate treatment and treatment of various industrial wastewaters [3–7]. Therefore, membrane processes play an effective role in ensuring access to clean water for more people, sustainable use of water resources, and control of water pollution [8]. Polymeric membranes are more prevalent in large and small-scale water treatment applications due to simplicity of manufacturing, processability, flexible structures, and economic feasibility [9]. Polyethersulfone (PES) is commonly selected as a base material for membrane fabrication owing to its low fabrication cost and favorable processing characteristics [10,11]. Although PES is

1

^{*}Corresponding author/Yazışılan Yazar

widely utilized for fabricating porous microfiltration (MF) and ultrafiltration (UF) membranes, its greatest disadvantage is its tendency to fouling during filtration [12]. Fouling of polymerbased membranes such as PES membranes triggers the flux reduction problem, which is a very common problem during membrane filtration. Various modification techniques—including blending, surface grafting, chemical treatment, and surface coating—are applied to improve the characteristics and fouling resistance of polymer-based membranes. Blending, one of the membrane modification techniques, stands out as a widely used method due to its simplicity, the absence of complex chemical processes, and its applicability to low-molecular-weight polymers [13].

Cellulose acetate (CA) is extensively employed in membrane fabrication owing to its capability to form uniform membrane structures from renewable raw materials, high hydrophilicity, biodegradability, solvent resistance, and tolerance to chlorine concentrations up to 1 ppm [14]. Pure membranes produced from three different polymers, 16 wt% CA, 16 wt% PES and 16 wt% polyvinylidene fluoride (PVDF), were compared, and it was determined that the active surface of the CA membrane was more hydrophilic than the other membranes [18]. A study found that the pure water flux (PWF) of the CA membrane at 1 bar (462.2 L/m²·h) was significantly higher than that of the PES membrane (19.2 L/m²·h) and the PVDF membrane (79.3 L/m²·h) [15]. Since the hydroxyl groups in the chemical structure of CA increase its affinity for water, blending more hydrophobic polymers [13], such as PES, with CA can improve membrane water flux performance and antifouling capabilities by improving the hydrophilicity of membranes. For instance, a study showed that the PWF of PVC/PES membrane increased from 150.5 L/m².h to 1482.1 L/m².h by incorporating 5%-30% CA into polyvinyl chloride (PVC)/PES blend membrane [16]. By mixing CA into the PVC/PES membrane, the contact angle of the membrane also decreased, and the membrane surface became more hydrophilic [16]. Similarly, in a study by Liu et al., the contact angle of the membrane decreased, and the hydrophilicity of the membrane improved with the addition of CA to the PES-based membrane [20]. Liu et al. reported that for membranes produced by reverse thermally induced phase separation method, when the amount of CA in the casting solution was 0.5 wt% and the membrane formation temperature was 323K, the PWF and bovine sebum albumin (BSA) rejection rate increased by 48.9% and 23.6%, respectively, compared to pure PES membrane [17].

CNCs and CNFs are nanocellulose species derived from cellulose, just like CA. CNCs are usually produced by strong acid hydrolysis, while CNFs are produced by mechanical methods [18]. In addition to the difference in production methods and crystallinity between CNCs and CNFs, there is also a difference in size, with CNFs being longer than CNCs [18,19]. CNCs and CNFs have been used by many researchers as reinforcement materials in polymeric membrane structures due to their small size, high aspect ratio, high specific surface area, high strength and hydrophilic nature. The results of studies revealed that CNCs and CNFs changed the morphology [20,21], improved the surface hydrophilicity [20,22], enhanced the flux performance [20–23], improved the mechanical properties [21,23], and increased the fouling resistance of membranes [20,23].

In this study, the effect of 0.5 wt% nanocellulose reinforcements on the polymer matrix consisting of 15 wt% PES-CA (90/10 wt%) blend was investigated on the structural properties, flux performance, turbidity rejection percentage, antifouling ability, and fabrication cost of the membrane. To increase the affinity of the PES membrane, which is known for

its high hydrophobicity and tendency to fouling, to improve its flux performance and to increase its resistance to fouling, PES was blended with cellulose-derived polymer (CA) and nanomaterials (CNC and CNF) containing abundant hydroxyl (-OH) groups. The findings from this study may contribute to further improvements in the performance of PES-based membranes produced using cellulose-based materials/nanomaterials in future studies.

2 Materials and methods

2.1 Materials used in the membrane fabrication

PES Veradel 3000P, CA, and 1-Methyl-2-pyrrolidone (NMP) were obtained from Solvay, Sigma Aldrich, and Merck, respectively. CNF and CNC were obtained from Nanografi, Türkiye. Table 1 shows the properties of the chemicals used in membrane fabrication. Purchased chemicals were used in membrane fabrication studies without further purification. Purchased CNC was produced by sulfuric acid hydrolysis and purchased CNF was mechanically processed after modification by carboxymethylation. The raw materials for CNC and CNF were pine wood and cotton, respectively. Figure 1 shows the scanning electron microscope (SEM) images of the powdered forms of CNC and CNF used in the membrane fabrication.

Table 1. Materials used in flat sheet membrane fabrication.

Table 1. Materials asea in flat sheet membrane labiteations		
Material	Properties	
11/0	Form: Powder	
PES	Mw: ~63,000 g/mol	
	Form: Powder	
	Mn: ~50,000 g/mol	
CA	Impurities: ≤3% water	
NMP	Purity: 99.5%	
	Form: Powder	
	Color: White	
CNF	Moisture: ~4 wt.%	
	Diameter: 0.01–0.02 μm	
	Form: Powder	
	Color: White/off white	
CNC	Moisture: <6%	
	Diameter: 0.01–0.02 μm	



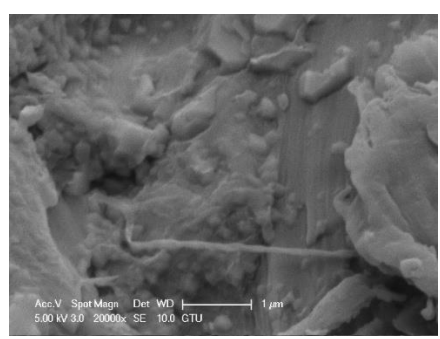


Figure 1. SEM images of (a) powdered CNC and (b) powdered CNF.

2.2 Fabrication of nanocomposite flat sheet membranes

Membranes containing 13.5 wt% PES and 1.5 wt% CA were fabricated using the non-solvent induced phase separation technique, which is widely preferred for the preparation of membranes (Figure 2). The total polymer ratio in the membranes was 15%. PES and CA accounted for 90% and 10% of the total polymer content of the membranes, respectively. The constituent ratios of the casting solutions used in producing polymeric membranes are listed in Table 2. NMP (solvent) was added to 250 mL heat-resistant bottles, and the solvent was stirred at 60 °C for 2 min. Then CA and PES were added to the glass bottle, respectively. The PES/CA/NMP solution was stirred at 60 °C for 24 h until a homogenous solution was formed. Then, ultrasonic degassing was performed in a water bath at 25 °C for 30 min. The prepared solution was cast onto a well-dried glass plate and then spread onto the glass plate with a thickness of 200 µm. Immediately following this step, the glass plate was submerged in a distilled water coagulation bath. The temperature of the coagulation bath was 25 °C. Membranes were formed by exchange between the NMP and the distilled water. The produced membranes were kept in plastic containers with lids filled with distilled water at room temperature in a light-proof cabinet until membrane characterization studies. The fabrication of PES/CAbased membranes blended with CNC and CNF was carried out with a procedure similar to the fabrication procedure of PES/CA membranes.

Table 2. The constituent ratios of the membrane casting solutions.

	PES (wt.%)	CA (wt.%)	NMP (wt.%)	CNC (wt.%)	CNF (wt.%)
PES/CA	13.5	1.5	85	-	-
PES/CA/CNC	13.5	1.5	84.5	0.5	-
PES/CA/CNF	13.5	1.5	84.5	-	0.5



Figure 2. Membrane fabrication process.

2.3 Hansen solubility parameters (HSPs) for membrane components

Hansen solubility parameters (HSPs) offer a quantitative framework for assessing the solubility behavior of polymers in specific solvents [24]. HSPs are based on the principle that polymers dissolve in solvents with similar properties [25]. HSPs are designed to understand the effect of molecular structure on solubility [26]. The HSPs approach was applied to optimize solvent selection, identify the solvent providing the highest polymer solubility in the casting solution, and investigate the influence of component interactions on the final membrane structure [9,27]. The total solubility parameter (δ_t) is the combination of the three components of a molecule, taking into account dispersion force (δ_{d}) polar force (δ_{p}) , and hydrogen bonding (δ_h) interactions (Equation 1) [28].

$$\delta_t = \left| \delta_d^2 + \delta_p^2 + \delta_h^2 \right| \tag{1}$$

Figure 3 shows the HSPs of polymers (PES and CA), solvents (NMP, DMF, DMAc, DMSO, and THF), and nonsolvent (water).

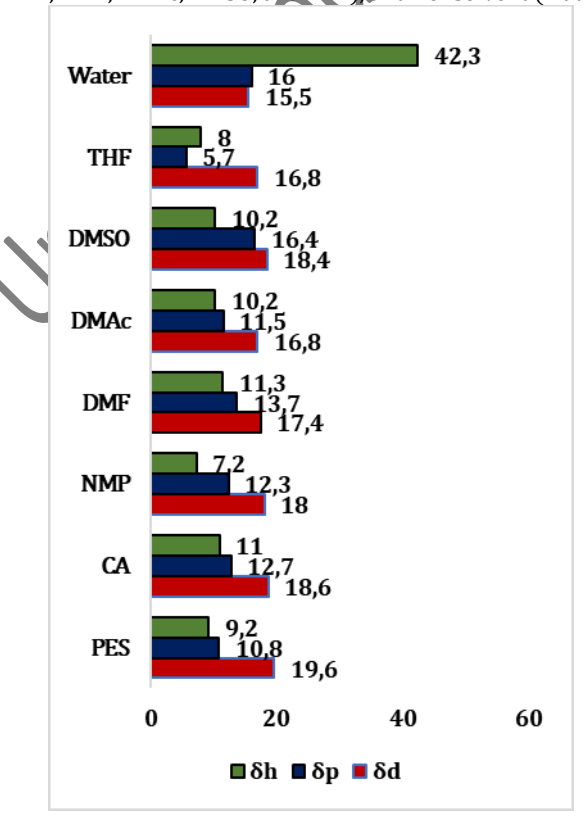


Figure 3. HSPs of polymers, solvents, and water [28]. The compatibility of polymer and solvent can be analysed using the HSP distance (Ra). Ra is calculated using Equation 2 [28].

$$Ra = \sqrt{4(\delta_{d1} - \delta_{d2})^2 + (\delta_{p1} - \delta_{p2})^2 + (\delta_{h1} - \delta_{h2})^2}$$
 (2) where Ra is the distance between the solvent and the polymers.

 δ_{d_t} δ_{p_t} and δ_{h} represent the hydrogen bonding component, polar component, and dispersion component of the HSP, respectively. 1 represents the solvent, and 2 represents the other component (polymer or nonsolvent (water)).

HSPs for a blend membrane ($\delta_{d,blend}$, $\delta_{p,blend}$, and $\delta_{h,blend}$) are calculated using the fraction of components and solubility parameters of pure polymers (Equations 3-5) [29].

$$\delta_{d,blend} = \delta_{d,1}\phi_1 + \delta_{d,2}\phi_2
\delta_{p,blend} = \delta_{p,1}\phi_1 + \delta_{p,2}\phi_2$$
(3)

$$\delta_{n\,hlend} = \delta_{n\,1}\phi_1 + \delta_{n\,2}\phi_2 \tag{4}$$

$$\delta_{h,blend} = \delta_{h,1}\phi_1 + \delta_{h,2}\phi_2 \tag{5}$$

The symbols ϕ_1 and ϕ_2 define the volume contributions from component 1 and component 2.

Membrane characterization

The functional groups of the membranes were investigated by Fourier Transform Infrared (FTIR) spectroscopy using an FTIR spectrophotometer.

Prior to SEM imaging, the membranes were air-dried at room temperature and sputter-coated with a thin layer of gold (10 mA, 90 s). Surface morphology was then examined at magnifications of $5000 \times$ and $20000 \times$.

Atomic force microscopy (AFM) was conducted to quantitatively assess the membrane surface roughness, providing measurements R_a, R_q, R_z, and R_{max}.

X-ray diffraction (XRD) of membranes were recorded within the 2θ range of 3–70°.

Membrane water content was measured by oven-drying (45 °C, 60 h), short-term immersion in distilled water (1 min), blotting, and subsequent calculation using Equation 6 based on the wet (W_w) and dry weights (W_d) of the membranes [30]. $Water\ content = \frac{Ww - Wd}{Ww} \times 100$

$$Water content = \frac{Ww - Wd}{Ww} \times 100$$
 (6)

The porosity (P) and average pore size (rm) of the membranes were calculated using Equations 7 and 8, respectively [30].

$$P = \frac{W_w - W_d}{A \, l \, \rho} \, x \, 100 \tag{7}$$

where, A, l, and ρ represent the membrane surface area (cm²), membrane thickness (cm), and density of water, respectively.

$$rm = \sqrt{\frac{(2.9 - 1.75P) \times 8\eta lQ}{P \times A \times \Delta P}}$$
 (8)

where, η , l, and Q represent the viscosity of water (Pa.s), membrane thickness (m), and permeate volume per unit time (m³/s), respectively. A and ΔP represent the effective membrane area (m2) and operating pressure of the filtration system (3 bar), respectively.

Evaluation of membrane pore characteristics using 2.5

The SEM surface image of the membrane can be analyzed in MATLAB to determine the porosity, pore size distribution, and average pore size of the membrane. In this study, the reasons for analysing the pore structure characteristics of membranes from SEM images with a MATLAB script can be listed as follows: $(1) \ \ \text{MATLAB} \ is \ capable \ of \ precisely \ analysing \ the \ porosity \ and$ pore size in the image by examining the SEM images in detail. (2) MATLAB's automated measurement capabilities, enabled by image processing algorithms, yield more precise results by reducing the potential for errors inherent in manual measurement. (3) The rapid application of image processing algorithms in MATLAB allows for comprehensive image analysis in a relatively short time, thereby saving time. SEM images at 20,000× magnification were analyzed with MATLAB to evaluate membrane surface porosity and pore dimensions [31,32].

In the first stage, Fiji software was used to determine how many pixels correspond to the scale bar located at the bottom centre of the original SEM images. The total width of the original SEM images and the widths of the scale bars representing 1 μm were determined as 1424 pixels and approximately 231 pixels, respectively. The ratio of the determined pixel values was used as a variable in the "resolution" parameter in the MATLAB script. The MATLAB script was run and visual results of depth map, binary map, pore segmentation map and pore size distribution were obtained from the original SEM image for each membrane. The following steps were performed respectively in the analysis of the SEM images of the membranes using the MATLAB script in MATLAB:

Original SEM images: Grayscale SEM images in jpg format with 20000x magnification were used as initial data for the analysis. In the resolution section of the script, a variable calculated based on pixels representing the width of the image and the length of the scale bar was entered.

Depth maps: Maps were created to determine the depth of the pores in the SEM images by image processing techniques.

Binary maps: The pores in the SEM images were highlighted in order to easily analyse the number and size of the pores. For this purpose, the pores and the solid phase (non-porous parts of membranes) in the SEM images were separated in the binary maps. Pores were visualised in black colour and the solid phase $% \left(1\right) =\left(1\right) \left(in white colour.

Pore segmentation maps: Pore segmentation maps contribute to determining the number and size of pores. Pores in the SEM images were segmented. Pores are individually identified and

labelled in this map. **Pore size distribution:** Pore diameter distribution histograms show the distribution of pores by diameter in SEM images of membranes. At this stage, for each pore in the segmentation map, its size was calculated and the size of the pores was presented as histograms.

In addition to the visual results, the porosity value (fraction) of the membrane and the average pore size with standard deviation were also calculated in MATLAB.

Testing of membrane permeation and separation efficiency

The water flux performance of the membranes was examined in a dead-end membrane filtration setup at 3 bar. Figure 4 shows a dead-end membrane filtration setup for filtering distilled water/lake water through flat sheet membranes. Nitrogen gas was used as the driving force to supply a pressure of 3 bar for filtering water through the membranes. No heater was used in the flux tests, and the tests were carried out at room temperature. Membrane samples were positioned inside the dead-end filtration cell. The dead-end filtration cell with a capacity of approximately 0.3 L was filled with distilled water or surface water. A magnetic apparatus was also included in the dead-end filtration cell to ensure continuous mixing. The filtration cell containing distilled and surface water was continuously stirred while positioned on a magnetic stirrer. Membrane permeate weight-time graphs were obtained by means of a cable connected to the precision balance and computer, and the RSweight software. The flux values (L/m².h) of the membranes were calculated from the weight-time data obtained. Water flux values of the flat-sheet membranes were calculated according to Equation 9 [30].

$$J = \frac{V}{A \times \Delta t} \tag{9}$$

where, I, V, A, and Δt represent the flux (L/m²·h), permeate volume (L), membrane area (m²), and filtration time (h). Distilled water flux (Jw1) and surface water (Terkos Lake water) flux (Js) of the produced membranes were investigated. The surface water-filtered membranes (fouled membranes) were soaked in distilled water for 15 minutes to facilitate physical cleaning. In the following step, the water flux of the membranes after physical cleaning (Jw2) was measured using distilled water.

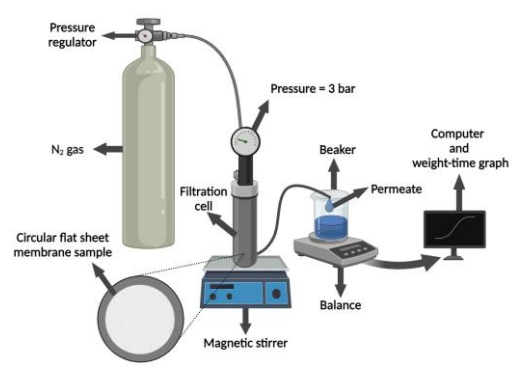


Figure 4. Dead-end membrane filtration setup.

The turbidity rejection of the produced membranes from the Terkos lake water was investigated by a dead-end filtration setup. Turbidity was measured using a turbidity meter (HACH 2100Q). The membranes' effectiveness in removing turbidity from surface water (R, %) was determined using Equation 10, taking into account the turbidity values in the feed (Cx, NTU) and permeate (C_{p_r} NTU).

$$R = \frac{c_f - c_p}{c_f} \tag{10}$$

Calculation of antifouling ability parameters of 2.7 membranes

Fouling ratios, flux recovery ratio (FRR) values and flux decay ratio (FDR) values were calculated to determine the antifouling ability of the membranes. Jw1, Js and Jw2 values obtained from the flux tests of the membranes were used in the equations below (Equations 11-15) [33, 36] to calculate the total fouling ratio (Rt), irreversible fouling ratio (Rir), reversible fouling ratio (Rr), FRR value and FDR value of the membranes.

ratue and FDR value of the memoranes.

$$R_{t} = \frac{J_{w1} - j_{s}}{j_{w1}} \times 100 \tag{11}$$

$$R_{ir} = \frac{j_{w2} - j_{s}}{j_{w1}} \times 100 \tag{12}$$

$$R_{r} = \frac{j_{w2} - j_{s}}{j_{w1}} \times 100 \tag{13}$$

$$FRR = \frac{j_{w2}}{j_{w1}} \times 100 \tag{14}$$

$$FDR = \frac{j_{w1} - j_{s}}{j_{w1}} \times 100 \tag{15}$$

$$FDR = \frac{j_{w1} - J_s}{j_{w1}} \times 100 \tag{15}$$

2.8 Resistance calculation

For the membranes, total hydraulic resistance (RT), membrane resistance (RM), as well as fouling-related resistances—namely irreversible (RIR) and reversible (RR) fouling resistances were calculated using Equations 16-20 [37]. RF is the fouling resistance. RF value is equal to the sum of RIR and RR.

$$RT = RM + RF \tag{16}$$

$$RM = \frac{\Delta P}{lw1 \times n} \tag{17}$$

$$RF = RIR + RR \tag{18}$$

$$RIR = {}^{\Delta P} RM \tag{19}$$

$$RIR = \frac{\Delta P}{Jw2 x \eta} - RM \tag{19}$$

$$RR = \frac{\Delta P}{Js x \eta s} - RIR - RM \tag{20}$$

$$RR = \frac{\Delta P}{Js \times \eta s} - RIR - RM \tag{20}$$

P, η , and ηs represent the pressure applied to the membrane (Pa), the viscosity of distilled water (Pa·s), and the viscosity of surface water (Pa·s), respectively.

3 Results and Discussion

3.1 Solvent selection for polymer-based membrane fabrication

A low Ra value indicates a high compatibility between polymersolvent, solvent-non/solvent or polymer-nonsolvent pairs, whereas a high Ra value indicates a low compatibility between these pairs. A low Ra value calculated for polymer-solvent indicates that the solvent is a good candidate to dissolve the polymer. On the contrary, a high Ra value indicates a lower dissolving capacity of solvent. Table 3 shows the calculated Ra values for polymer-solvent and solvent-nonsolvent pairs. The Ra values of PES-NMP, PES-DMF, PES-DMAc, PES-DMSO and PES-THF were 4.06, 5.67, 5.73, 6.17 and 7.67 MPa1/2, respectively. This indicated that among the solvents analysed, NMP had the strongest interaction with PES while THF had the weakest interaction. The Ra values of CA-NMP, CA-DMF, CA-DMAc, CA-DMSO and CA-THF were 4, 2.62, 3.88, 3.81 and 8.42 MPa1/2, respectively. Solvents are ranked according to their capacity to dissolve CA as follows: DMF > DMSO > DMAc >NMP > THF. The high *Ra* values of PES-Water and CA-Water, $34.49~MPa^{1/2}$ and $32.08~MPa^{1/2},$ respectively, indicate that water is not a good solvent for PES and CA, i.e. it is a nonsolvent. A solvent with a very low ability to dissolve the polymer, i.e. a nonsolvent, is selected to precipitate the polymer by solvent and nonsolvent exchange [33].

Since NMP was the best solvent among the solvent options for PES, which constituted the majority of the 15 wt% polymer content in the casting solutions planned to be prepared for the fabrication of membranes, NMP was used as the solvent in the casting solutions. Since water has a high Ra value for both PES and CA, indicating the low compatibility of both polymers with water, only water was used as a non-solvent in the phase inversion process. Also, it is worth noting that the Ra value calculated for NMP-water was higher than the Ra value calculated for other solvents-water, except THF-water, indicating that the compatibility between NMP and water was low. The low compatibility between solvent (NMP) and nonsolvent (water) indicates that the solubility parameters of the components are far from each other. This may allow for rapid exchange of NMP and water when the polymeric casting solution is immersed in water during phase inversion.

The calculated Ra values for PES/CA-NMP and PES/CA-water were 3.93 and 34.25 MPa/2, respectively. Similar to the compatibility between pure polymer-NMP and pure polymerwater, the Ra values for the PES/CA blend confirmed that NMP is a good solvent while water is a poor solvent. The Ra value for PES/CA-NMP was lower than that for PES-NMP, indicating that the compatibility for NMP increased with the addition of CA at the specified ratio to the membrane casting solution and that the PES/CA blend can be well solubilized in NMP. In addition, since the Ra value for PES/CA-Water was lower than that of PES-Water, it was determined that the compatibility of the polymer mixture in the membrane casting solution with water increased with the addition of CA, which has the potential to contribute to an accelerated phase inversion.

Table 3. Ra values for polymer-solvent and solvent-nonsolvent pairs.

	Ra
PES-NMP	4.06
PES-DMF	5.67
PES-DMAc	5.73
PES-DMSO	6.17
PES-THF	7.67
PES-Water	34.49
CA-NMP	4.00

CA-DMF	2.62
CA-DMAc	3.88
CA-DMSO	3.81
CA-THF	8.42
CA-Water	32.08
NMP-Water	35.65
DMF-Water	31.32
DMAc-Water	32.52
DMSO-Water	32.62
THF-Water	35.91
PES/CA-NMP	3.93
PES/CA-Water	34.25

3.2 Functional groups of membranes

Figure 5 shows the FTIR spectra. Peaks at about 1580 and 1480 cm⁻¹ corresponded to the C=C stretching vibration in the benzene ring. Peaks at 1240 cm⁻¹ in the FTIR spectrum of all membranes indicated ether linkage between phenyl groups. Peaks at 1100 and 1150 cm⁻¹ indicated the sulfone groups of PES [34]. Peaks at 717 cm⁻¹ were attributed to the C-H bending vibration of PES [35]. The FTIR spectrum of PES/CA membrane showed the presence of -OH originating from CA in the membrane with a peak at 3500-4000 cm⁻¹ [36]. The intensity of the peak at 2927 cm^{-1,} indicating the C-H stretching vibration increased with CNC and CNF reinforcement of the PES/CA membrane. Moreover, the enhanced peak intensity in the -OH stretching vibration region (4000-3500 cm⁻¹) resulting from the incorporation of nanocellulose types indicates the presence of hydrophilic nanomaterials rich in hydroxyl groups within the membrane structure.

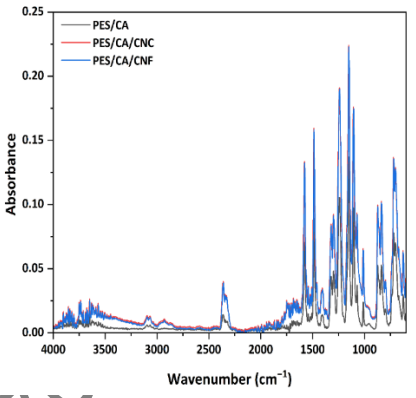


Figure 5. FTIR spectra recorded for membranes.

3.3 Surface morphology of membranes

Figure 6 shows SEM surface images of PES/CA-based membranes. When the SEM surface images at 500x magnification were evaluated, all of the PES/CA-based membranes produced by blending PES and CA polymers had circular collapses on the surface. The circular collapses on the surface of the PES/CA membrane were roughly in the range of 10-20 µm. The size of the circular collapses on the surface of the membrane decreased with CNC or CNF reinforcement of the PES/CA membrane. CNC reinforcement increased the number of circular collapses on the surface of the membrane while CNF reinforcement decreased it. SEM surface image results showed

that CNF is an effective reinforcement material for reducing the size and number of circular collapses on the surface of PES/CA membrane. When the relatively flatter surfaces of the membranes, which did not coincide with the depression region, were examined at high magnification, i.e. 20000x magnification, the surface of the PES/CA membrane was rougher than that of nanocellulose reinforced membranes. With CNC reinforcement of the PES/CA membrane, the surface roughness of the non-collapse regions of the membrane decreased and the non-collapse regions of the membrane became relatively smoother. Among the membranes produced, the membrane with the smoothest surface was PES/CA/CNF incorporation of CNC and CNF into the membrane matrix led to a noticeable reduction in the diameter of circular surface defects and contributed to a smoother membrane surface morphology.

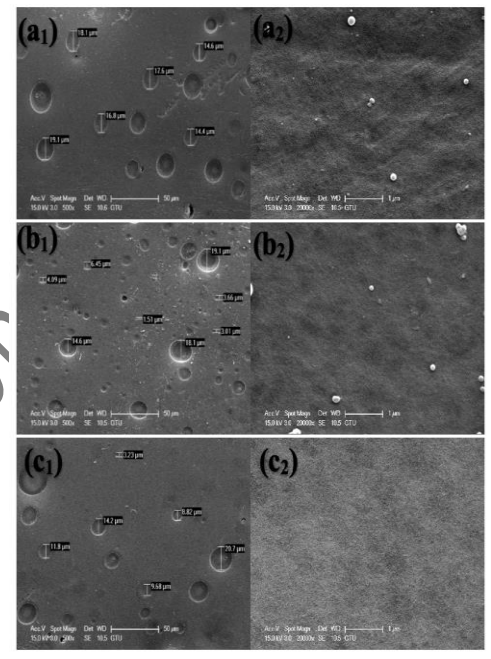


Figure 6. SEM surface images of membranes: (a) PES/CA, (b) PES/CA/CNC and (c) PES/CA/CNF. (1) and (2) are SEM images at 500x and 20000x magnification, respectively.

3.4 Analysis of porosity and pore size in membrane SEM images with MATLAB

The number and size of small pores in high magnification SEM surface images can be examined in detail using software. The effect of nanocellulose reinforcements on the number and size of small pores on the surface of PES/CA membrane, which cannot be easily observed under low magnification but can be observed at 20000x magnification, was analyzed in MATLAB with MATLAB script. Figure 7 (a), (b), (c) shows the original images, depth maps, binary segmentation maps, pore space segmentation maps and pore size distribution histograms of the SEM surface images of the membranes analyzed using MATLAB script. The analysis results showed that the porosity of PES/CA, PES/CA/CNC and PES/CA/CNF membranes were 30.84%, 16.891% and 0.10%, respectively. The average pore radius for PES/CA, PES/CA/CNC and PES/CA/CNF membranes were 0.62 ± 0.40 , 0.55 ± 0.30 and 0.33 ± 0.05 nm, respectively. Both porosity and average pore size decreased with CNC and CNF reinforcement of the PES/CA membrane under high magnification in the part of the membrane that does not contain large pores but contains very small pores. Considering the binary segmentation maps, the porosity in the part of the membrane containing small pores decreased very significantly and the solid phase of the membrane increased significantly with CNF reinforcement of PES/CA membrane (Figure 7 (a) and (c)). Furthermore, the average pore size of the small pore sizes observed under 20000x magnification of the PES/CA membrane was reduced by 50% with CNF reinforcement of the PES/CA membrane. The pore size scatter plots showed that the majority of the pores in the section of PES/CA, PES/CA/CNC and PES/CA/CNF membranes containing small pores under high magnification were roughly below 2, 1.5 and 0.5 nm. The results obtained from the analysis showed that: (1) CNC and CNF significantly reduced both the number and size of small pores observed under high magnification of PES/CA membrane, and (2) CNF was more effective than CNC in reducing the number and size of small pores of PES/CA membrane.

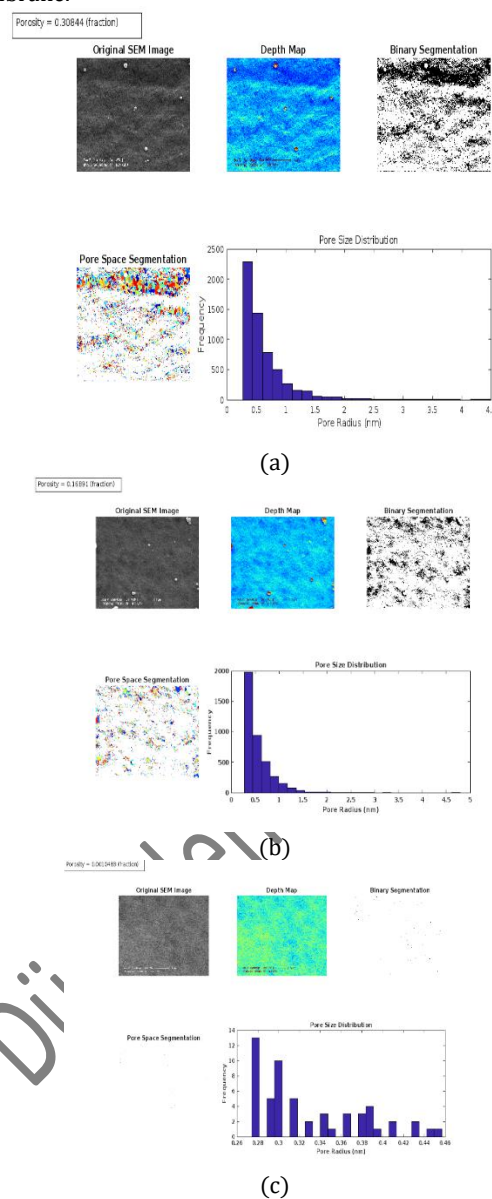


Figure 7. Analysis of porosity and pore size from SEM surface images of membranes in MATLAB: (a) PES/CA, (b) PES/CA/CNC and (c) PES/CA/CNF

3.5 Roughness Characteristics of Membrane Surfaces

AFM analysis was performed to investigate the surface roughness of the membranes and to determine the roughness parameters. Figure 8 shows two-dimensional and threedimensional AFM images of the membranes. Light regions and dark regions show peaks and valleys, respectively, in AFM images [37]. As seen from Figure 8, the surface of the PES/CA membrane was quite rough, and the surface roughness of the PES/CA membrane was significantly reduced by CNC and CNF reinforcement. The interaction between the membrane surface and the foulant plays a crucial role in the adhesion of foulants from the feed onto the membrane surface [38,39]. Table 4 shows the values of the roughness parameters of the membranes. PES/CA membrane had the highest values for all roughness parameters. R_a , R_q , R_z , and R_{max} values of the PES/CA membrane were 5.290, 8.290, 35.227, and 58.895 nm, respectively. Rough membrane surfaces are ideal for foulants in the feed to be trapped and accumulated in the valleys [40]. $R_{\text{a}\text{,}}$ $R_{\text{q,}}$ $R_{z,}$ and $R_{\text{max}}\,\text{values}$ of the membrane decreased with both types of nanocellulose reinforcement to the PES/CA membrane. The membrane with the lowest values in terms of all roughness parameter values was PES/CA/CNF. R_a , R_q , R_z , and R_{max} values for the PES/CA/CNF membrane were 3.356, 4.494, 20.266, and 27.345 nm, respectively. Similarly, the roughness parameters of CNF-reinforced PVDF membrane were reported to be lower than those of CNC-reinforced PVDF membrane [41].

The PES/CA blend membranes in this study were smoother than pure PES membranes. For instance, in a study by Tshabalala et al. AFM analysis result of 20 wt% PES-based membranes showed that the R_a and R_q values of the flat sheet membrane were 11.48 and 18.73 nm, respectively [42]. In the study by Krishnamoorthy and Sagadevan, the Ra value of 15 wt% PES-based flat sheet membrane produced by phase inversion was 53.76 nm [43]. Since the surface of the PES/CA membrane is smoother than that of the PES membrane reported in the literature [42–45], mixing 13.5 wt% PES with a low amount CA (1.5 wt.%) may contribute to reducing the potential for attachment of foulants to the membrane surface. In addition, AFM analysis revealed that especially the CNF type of nanocellulose is preferable for further reduction of the roughness of the PES/CA flat sheet membrane.

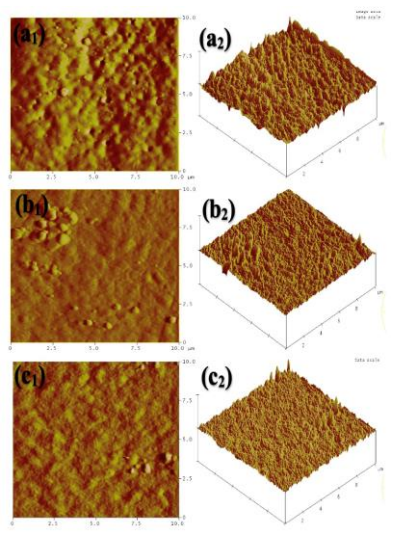


Figure 8. Two-dimensional (1) and three-dimensional (2) AFM images of the membranes: (a) PES/CA, (b) PES/CA/CNC and (c) PES/CA/CNF.

Table 4. Surface roughness characteristics of the membranes.

Membrane	Ra	R_{q}	Rz	R _{max}
PES/CA	5.290	8.290	35.227	58.895
PES/CA/CNC PES/CA/CNF	5.033 3.356	6.713 4.494	26.524 20.266	47.020 27.345

3.6 XRD patterns of membranes

Figure 9 shows the XRD patterns of the membranes. Sharp peaks in XRD patterns are indicative of the membrane's crystalline structure, whereas broad peaks correspond to its amorphous structure. In previous studies investigating the XRD patterns of PES membranes, it was reported that PES membranes have amorphous properties [46,47]. Since CA is a semi-crystalline polymer [48], XRD patterns of flat sheet membranes produced by mixing PES and CA polymers prepared in this study showed that the membranes were semicrystalline. The XRD analysis of the PES/CA membrane revealed diffraction peaks at 2θ values of 9.45°, 14.08°, 16.94°, 18.54°, 25.62°, and 28.62°, with the most intense peak observed at 16.94°. The XRD profiles of membranes reinforced with nanocellulose exhibited diffraction peaks comparable to those observed in the PES/CA membrane. Incorporation of CNC into the PES/CA membrane resulted in the appearance of two additional sharp peaks of low intensity at $2\theta = 56.67^{\circ}$ and 57.12° in the XRD pattern. The change observed in the XRD pattern upon CNC addition is attributed to the crystalline nature of CNC, confirming its presence in the membrane. In contrast, the addition of CNF to the PES/CA membrane did not result in the appearance of any new diffraction peaks. The higher crystallinity of CNC compared to CNF, which contains only crystalline regions in its structure, caused a significant change in the XRD pattern.

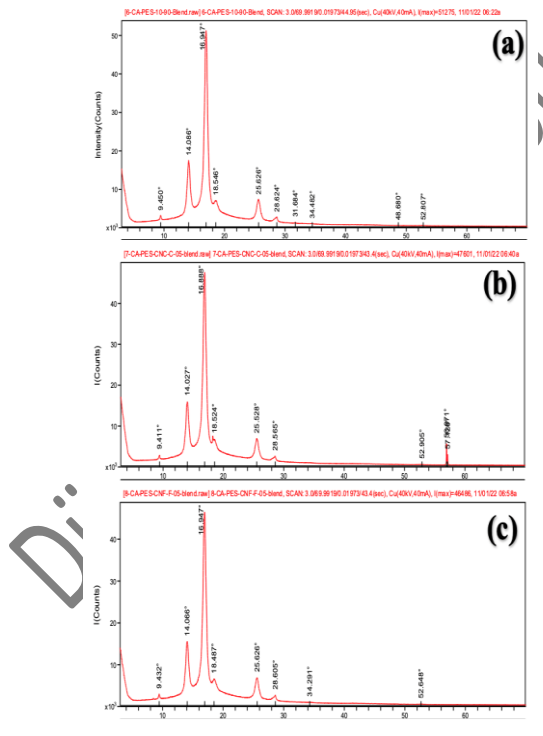


Figure 9. XRD patterns of membranes: (a) PES/CA, (b) PES/CA/CNC, and (c) PES/CA/CNF.

3.7 Hydrophilicity and pore structure of membranes

Membrane water content, often referred to as water uptake, serves as an indicator of the hydrophilic properties of membranes. The PES/CA membrane exhibited a water content of $63.10\pm8.58\%$. Incorporation of 0.5 wt% CNC and 0.5 wt% CNF enhanced the water content to $66.87\pm5.18\%$ and $70.39\pm2.31\%$, respectively (Figure 10(a)). The presence of abundant hydrophilic hydroxyl groups in CNC and CNF enhanced the interaction between the membrane and water, thereby increasing the membrane's water content. The water content analyses of the membranes showed that the hydrophilicity of the PES/CA membrane increased with CNC and CNF reinforcement. Similarly, Zhang et al. observed that incorporating 5 wt% CNC into a membrane composed of 15 wt% PES and 2 wt% PVP increased its water content from 54 to 70 wt%, with the hydrophilic CNC, rich in free hydroxyl groups, enhancing the membrane's hydrophilicity [49].

The structural characteristics of membranes, particularly porosity and average pore dimensions, play a key role in determining flux and separation performance. Membranes with reduced porosity and narrower pores exhibit lower water permeability under identical operating conditions, whereas those with higher porosity and larger pores facilitate water transport more efficiently. Figure 10(b) presents the porosity and mean pore size of the membranes. The base PES/CA membrane exhibited a porosity of 19.96 \pm 6.47%, which increased to 28.33 \pm 6.41% and 30.29 \pm 2.15% upon the addition of CNC and CNF, respectively. This enhancement in porosity can be explained by two factors. First, incorporating hydrophilic nanocellulose into the polymer matrix may generate localized stress points, promoting the formation of pores within the membrane structure [50]. Secondly, hydrophilic nanocellulose affects the stability of the polymer solution, accelerating solvent-non-solvent exchange and thereby influencing pore formation during the phase separation [22,50]. The formation of fracture points on the membrane surface and the increase in the liquid-liquid demixing rate during phase inversion lead to the formation of a more porous membrane structure. On the other hand, the average pore size of the PES/CA membrane, which was 12.52±3.38 nm, decreased slightly with the addition of CNC and CNF to the membrane. The average pore size of PES/CA/CNC and PES/CA/CNF membranes was 11.82 ± 2.26 and 11.49 ± 1.18 nm, respectively. The average pore sizes of the membranes were greater than 1 nm but smaller than 100 nm, confirming their classification as ultrafiltration (UF) membranes. Thanks to their small pore size, UF membranes can remove suspended solids, turbidity. oil-grease, organic matter, microorganisms from water and wastewater with high efficiency [51]. Therefore, the UF membranes with average pore sizes smaller than 13 nm produced in this study have the potential to be used in the physical separation of pollutants larger than 13 nm by size exclusion mechanism.

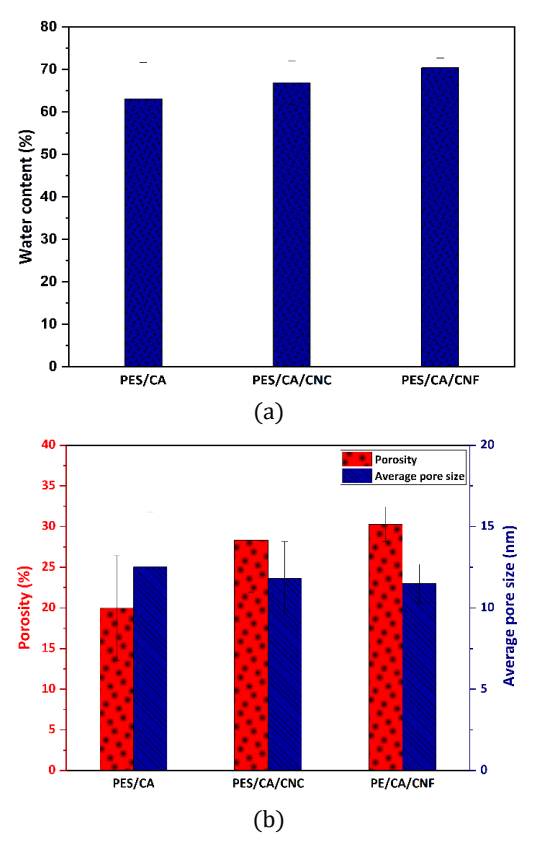


Figure 10. (a) Water content of membranes and (b) porosity and average pore size of membranes.

3.8 Water flux and turbidity rejection performance of membranes

Membranes with high selectivity as well as high flux performance are ideal for water and wastewater treatment. Membranes with high water fluxes provide more filtered clean water (permeate) per unit time. Membranes with higher water flux values are also energy efficient, that is, they consume less energy in the filtration process. Membranes with higher flux values contribute to obtaining large volumes of clean water in less time, especially in large-scale treatment applications, such as water and wastewater treatment plants serving high populations.

Reinforcing PES/CA membranes with CNC and CNF resulted in higher water flux values (Jw1, Js, and Jw2) compared to the unreinforced membrane (Figure 11). The hydrophilic hydroxyl groups present in the nanocellulose enhanced membrane-water interactions, promoting water permeability. Structural characteristics, particularly porosity, further facilitated water transport, as the nanocellulose-reinforced membranes displayed increased porosity relative to the PES/CA membrane. This combination of improved hydrophilicity and porosity contributed to superior flux performance, with the PES/CA/CNF membrane demonstrating the highest flux values of 502.25, 463.72, and 484.31 L/m²·h for Jw1, Js, and Jw2, respectively.

Consistent with the present results, previous studies have shown that incorporating CNC or CNF into polymeric membranes enhances their water flux. For instance, Bai et al. (2020) observed that adding 0.3 g of CNC (equivalent to 2 wt% CNC relative to PES) to a PES/PVP membrane increased its water flux from 185 L/m²·h at 60 kPa to 291 L/m²·h [22]. Lv et al. (2018) reported that the PWF of an unmodified PVDF

membrane at 100 kPa was 9.8 L/m²·h. They found that incorporating CNF in the range of 0.8 wt% to 4.2 wt% progressively enhanced the membrane's water flux, reaching 206.9 L/m²·h for the PVDF membrane reinforced with 4.2 wt% CNC [50]. In a study investigating the flux performance of polysulfone-based membranes at pressure values in the range of 3-7 bar, it was reported that the water flux performance increased as the CNF addition to the polysulfone-based membrane increased (from 0.1% to 0.5%) [52].

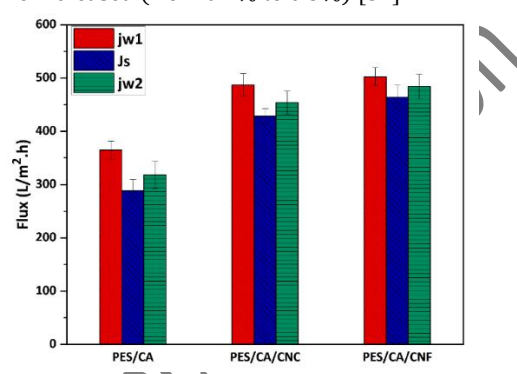


Figure 11 Water flux of membranes.

Table 5 shows the turbidity rejection percentage of PES/CAbased membranes from Terkos Lake water. The turbidity removal of PES/CA, PES/CA/CNC, and PES/CA/CNF membranes from lake water was 95.46%, 97.82%, and 98.24%, respectively. The turbidity rejection of nanocellulosereinforced PES/CA blend membranes improved as a result of the reduced average pore size induced by nanocellulose incorporation, which hindered the passage of solids present in lake water. In water treatment applications, achieving both high flux and high contaminant removal performance in membranes is highly desirable. Generally, increased porosity enhances water flux but tends to reduce contaminant removal efficiency. However, in this study, despite the increased porosity resulting from the incorporation of nanocellulose into the PES/CA membrane, the reduced average pore size contributed to an improvement in turbidity rejection performance. Consequently, a dual advantage was achieved, providing both high flux and high removal performance. Among the membranes produced, the PES/CA/CNF membrane exhibited high water flux performance as well as high turbidity removal efficiency from lake water, indicating that PES/CA/CNF is the most ideal membrane for water filtration applications.

Table 5. Turbidity rejection percentage of membranes.

,	
Membrane	Turbidity rejection
	percentage (%)
PES/CA	95.46
PES/CA/CNC	97.82
PES/CA/CNF	98.24

3.9 Antifouling ability of membranes

Figure 12 shows the fouling parameters of the membranes. The PES/CA membrane exhibited an Rt value of 21.02%, which was reduced upon the incorporation of CNC and CNF reinforcements. Nanocellulose-reinforced PES/CA membranes had better antifouling performance, as a lower Rt indicates that the membrane has better antifouling performance. This can be explained by the lower surface roughness value of CNC and CNF

reinforced nanocomposite PES/CA membranes compared to PES/CA membrane.

Rir values of PES/CA, PES/CA/CNC, and PES/CA/CNF membranes were 12.77%, 6.87% and 3.57%, respectively, while Rr values were 8.24%, 5.21% and 4.09%, respectively. The Rt (7.67%) and Rir (3.57%) values of the CNF reinforced PES/CA membrane were lower than those of other membranes. Furthermore, the analysis of fouling contributions revealed that the Rir component accounted for the largest proportion of the Rt in both PES/CA and PES/CA/CNC membranes, whereas the Rr component was dominant in the PES/CA/CNF membrane. These results indicate that the incorporation of nanocellulose enhanced the membranes' resistance to fouling, with CNF demonstrating a superior effect in improving the antifouling performance of the PES/CA membrane compared to CNC.

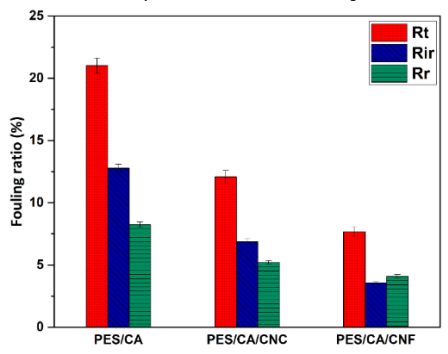


Figure 12. Fouling parameters of membranes.

Figure 13 presents the values of the FRR and FDR for membranes. Membranes with high FRR values experience less flux loss compared to the initial performance and high FRR value is an indication of the superior antifouling properties of the membranes. PES/CA membrane had the lowest FRR value with 87.22%. When CNC and CNF were incorporated into the PES/CA membrane, the FRR value increased to 93.12% and 96.42%, respectively. The addition of CNC and CNF to the PES/CA membrane enabled the flux loss due to fouling and clogging of the PES/CA membrane to be recovered more after the cleaning process. The higher FRR value of CNC and CNF reinforced nanocomposite PES/CA membranes compared to PES/CA membrane showed that these membranes operated with a flux performance closer to the initial performance after cleaning.

Since the FDR value is an indicator of flux decay, lower FDR values indicate that the membranes are more resistant to fouling. While the FDR value of the PES/CA membrane was 21.02%, the FDR value of the membrane decreased to 12.08% and 7.67% with CNC and CNF reinforcement, respectively. The lower FDR value of nanocellulose reinforced PES/CA membranes compared to PES/CA membrane indicated that nanocellulose reinforced membranes were less clogged during filtration and the flux performance was more stable. Considering the fouling ratio parameters, FRR value and FDR value as indicators of antifouling ability, PES/CA/CNF membrane had the most superior antifouling ability.

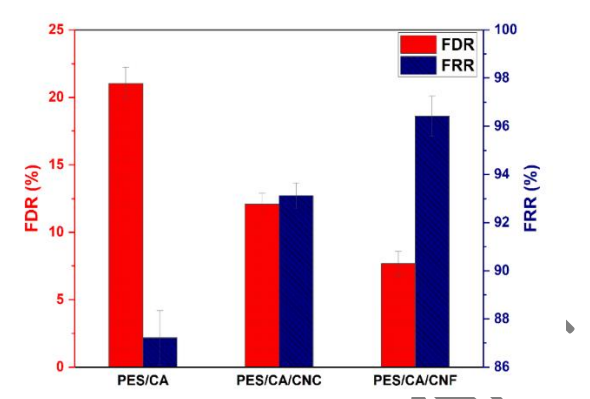


Figure 13. FRR and FDR values of membranes

3.10 Resistance calculations

Figure 14 (a) and Figure 14 (b) show the different types of resistance calculated for the membranes and the contribution of the different types of resistance to the total resistance, respectively. The RM values of PES/CA, PES/CA/CNC and PES/CA/CNF membranes were 3.32 x 10^{12} , 2.49×10^{12} and $2.42 \mathrm{x} 10^{12}~m^{\text{--}1}$ respectively and their contributions to the total membrane resistance (RT) were 78.97%, 87.91% and 92.32% respectively. The fact that the RM value constituted a significant part of the RT value of the membranes showed that a significant part of the hydraulic resistance was due to the physical properties of the membranes themselves. The RM value of PES/CA membrane decreased by 25.08% and 27.30% with CNC and CNF reinforcement, respectively. The reduced RM observed in nanocellulose-reinforced membranes, relative to the PES/CA membrane, can be attributed to their higher porosity compared to that of the PES/CA blend membrane. RIR and RR are the resistances caused by irreversible and reversible fouling, respectively. The RIR values of PES/CA, PES/CA/CNC and PES/CA/CNF membranes were 4.87x1011, $1.84x10^{11}$ and $8.95x10^{10}$ m⁻¹, respectively, while the RR values of the membranes were $3.98x10^{11}$, $1.59x10^{11}$ and $1.11x10^{11}$ m ¹, respectively. RIR values contributed more to the RT values of PES/CA and PES/CA/CNC than RR values. However, the contribution of RR (4.23%) to the RT value of CNF reinforced PES/CA membrane was higher than that of RIR (3.42%). The results showed that the effect of fouling resistance on the total resistance of PES/CA/CNF membrane was lower than other membranes and could be easily eliminated since most of the resistance caused by total fouling in PES/CA/CNF membrane was due to reversible fouling.

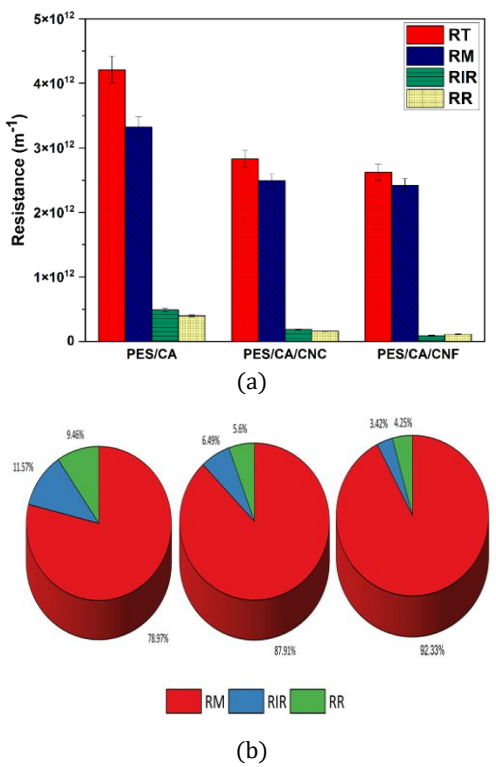


Figure 14 (a) Resistance of membranes and (b) Contribution of the different types of resistance to the total resistance.

3.11 Membrane fabrication cost

Table 6 shows the cost of chemicals used to produce the membrane casting solutions and the cost of electricity consumption used to produce the membranes in this study. Approximately 235.35, 332.46, and 393.97 Turkish liras (TRY) of materials were consumed to prepare 100 g of casting solution for the fabrication of PES/CA, PES/CA/CNC, and PES/CA/CNF membranes, respectively.

Table 6. Cost of chemicals and electricity consumed in membrane fabrication.

illeliibi alle labi leation.		
Material Cost		
PES	0.69 TRY/g	
CA	83.26 TRY/g	
NMP	1.19 TRY/mL	
CNC	195.40 TRY/g	
CNF	318.43 TRY/g	
Electricity Consumption Cost		
Magnetic stirrer with heater	0.6 kW x 24 h=14.4 kWh	
	14.4 kWh x 2.07 = 29.81 TRY	
Ultrasonic bath	$0.08 \text{ kW} \times 0.5 \text{ h} = 0.04 \text{ kWh}$	
	(for ultrasonic power)	
	$0.1 \text{ kW} \times 0.5 = 0.05 \text{ kWh (for }$	
	heater)	
110	Total = 0.09 kWh	
	$0.09 \times 2.07 = 0.1863 \text{ TRY}$	

*Electricity consumption fee is 2.07 TRY for 1 kWh.

 $15\, \rm flat$ sheet membranes of approximately 5 cm in width and $18\, \rm cm$ in length were produced from $100\, \rm g$ of casting solutions. In other words, membranes with a total area of $90\, \rm cm2$ were produced from $100\, \rm g$ of casting solution. It should be noted that the casting process in this study was performed manually using a casting knife. Therefore, to ensure that the casting process was not interrupted and to guarantee the fabrication of deformation-free membranes, a large amount of the polymeric

solution was poured onto the glass plate for each membrane fabrication. If a sufficient amount of polymer solution is not poured into the glass layer during the membrane casting process, tears may occur in some parts of the membrane in the casting process and membranes with less length are produced. For this reason, the excess casting solution overflowing out of the glass plate in the casting process was cleaned.

As for the electricity consumption, 14.4 kWh of energy was consumed when the magnetic stirrer with heater was used for the mixing of each solution for 24 h. After the stirring process, a total of 0.09 kWh of energy was consumed when the ultrasonic water bath with both heater and ultrasonic power was used for 30 min. Therefore, a total of 14.49 kWh of energy was consumed for the mixing and degassing of a membrane casting solution. In Turkey, the electricity consumption fee for 1 kWh is 2.07 TRY, up to a total of 240 kWh per month. Based on this information, the contribution of 14.49 kWh of energy consumption to the electricity bill is 29.99 TL. For the fabrication of 1 m² flat sheet PES/CA, PES/CA/CNC, and PES/CA/CNF membranes, the material costs (PES, CA, NMP, CNC, and CNF) are 1743.37, 2462.66, and 2918.33 TRY, respectively. For the fabrication of 1 m² membrane, assuming that the conditions for mixing the prepared casting solutions in a magnetic stirrer with a heater and degassing in an ultrasonic water bath are the same for 100 g of casting solutions, the electricity consumption cost will be 29.99 TRY. Therefore, the fabrication cost of 1 m² flat sheet PES/CA, PES/CA/CNC, and PES/CA/CNF membranes is 1773.66, 2492.65, and 2948.32 TRY, respectively. However, VAT is not included in this membrane fabrication cost, and electricity consumption is not based on industrial pricing. As a recommendation, performing the casting process using a device such as an automatic film applicator instead of manually can prevent the waste of polymer solution and contribute to the reduction of membrane fabrication cost. Although the fabrication of PES/CA blend membranes reinforced with CNC or CNF involves higher costs compared to unmodified PES/CA membranes, the superior water flux and enhanced antifouling properties of these nanocomposite membranes justify the additional expense. The improved water flux of CNC- and CNF-reinforced membranes enables the production of a greater volume of clean water in a shorter time, thereby reducing the energy demand during membrane operation.

4 Conclusion

In this study, PES/CA, PES/CA/CNC and PES/CA/CNF membranes were produced by the non-solvent induced phase separation method. The incorporation of CNC and CNF into the membranes led to an increase in both porosity and water content, while simultaneously reducing the average pore size and surface roughness of the membranes Analysis of highmagnification SEM images using a MATLAB script revealed that the addition of CNC and CNF further decreased the size of the smaller pores, and the local porosity was reduced in regions containing small pores. In the membrane process operated using a classical filtration technique, the PWF of the membrane composed of the PES and CA blend was 365.12 L/m²·h, which increased to 487.33 L/m²·h and 502.25 L/m²·h with the incorporation of CNC and CNF, respectively. In addition, the flux value of the membrane composed of the PES and CA blend for surface water increased from 288.34 L/m².h to 428.42 and 463.72 L/m².h with CNC and CNF reinforcement, respectively. CNC and CNF reinforcement not only improved the flux performance of the PES/CA membrane but also increased the turbidity rejection percentage and antifouling ability of the PES/CA membrane. Nanocellulose reinforcement decreased the Rt and FDR values of the PES/CA membrane, while increasing the FRR value, indicating that the nanocellulosereinforced nanocomposite membrane is more resistant to fouling. CNF reinforcement was more effective than CNC reinforcement in enhancing the antifouling ability of the PES/CA membrane, improving flux performance, and reducing surface roughness. Based on the costs of raw materials and electricity, the estimated fabrication cost for 1 m² of flat-sheet membranes was 1773.66 TRY for PES/CA, 2492.65 TRY for PES/CA/CNC, and 2948.32 TRY for PES/CA/CNF, excluding VAT. CNC and CNF reinforced PES/CA membranes had a higher fabrication cost, but it should be underlined that the higher performance of nanocellulose reinforced PES/CA membranes in both flux and fouling resistance may contribute significantly to the reduction of their operating costs.

Certain limitations of the present study also highlight opportunities for further investigation in future research:

- (1) It is worth noting that the water flow performance, removal efficiency, and fouling behavior of membranes vary depending on the feed type. In this study, water from Lake Terkos was used; therefore, it should be taken into consideration that tests conducted with different feed compositions may yield different results. This also presents an opportunity for future research.
- (2) Moreover, it is important to note that the short-term filtration performance of the membranes was investigated in this study. Future research could focus on evaluating their long-term performance, which would provide valuable insights into their applicability.
- (3) Another important consideration is that the incorporation of nanomaterials into polymeric membranes leads to changes in their chemical and mechanical stability. Therefore, future studies investigating the chemical resistance and mechanical properties (such as stress–strain curve, elastic modulus, tensile strength, and elongation at break) of CNC- and CNF-modified PES/CA membranes would represent an important step toward enhancing their applicability.

5 Author Contributions Statement

Author 1 contributed to the study by developing the concept, performing experiments, compiling the literature review, analyzing results, writing and editing the manuscript, and creating figures.

6 Approval by the Ethics Committee and Declaration of Conflict of Interest

This manuscript does not require approval from an ethics committee. The author declares that there are no conflicts of interest with any individual or institution related to this work.

7 References

- [1] United Nations. "The 17 Goals" https://sdgs.un.org/goals Accessed on 29 May 2025
- [2] Vajitha G, Jashrapuria K, Gandhi TP, Lipika P, Singh SP, Maliyekkal SM. "Scalable and cost-effective ultra-dispersible graphene oxide blended ultrafiltration mixed matrix membrane: Assessment of mechanical, water flux, and antibiofouling properties". Process Safety and Environmental Protection, 194, 35–46, 2025.
- [3] Li M, Luo J, Lu J, Shang W, Mu J, Sun F, et al. "A novel nanofibrous PAN ultrafiltration membrane embedded with ZIF-

- 8 nanoparticles for effective removal of Congo red, Pb(II), and Cu(II) in industrial wastewater treatment". Chemosphere, 304, 135285, 2022.
- [4] Manni A, Achiou B, Karim A, Harrati A, Sadik C, Ouammou M, et al. "New low-cost ceramic microfiltration membrane made from natural magnesite for industrial wastewater treatment". Journal of Environmental Chemical Engineering, 8(4), 103906, 2020.
- [5] Genç N, Durna E. "Determination of optimal method for management of leachate membrane concentrate by analytical hierarchy process". Pamukkale University Journal of Engineering Sciences, 26(3), 488–495, 2020.
- [6] Kamińska G, Marszałek A. "Advanced treatment of real grey water by SBR followed by ultrafiltration—Performance and fouling behavior". Water, 12(1), 154, 2020.
- [7] Ding H, Zhang J, He H, Zhu Y, Dionysiou DD, Liu Z, et al. "Do membrane filtration systems in drinking water treatment plants release nano/nicroplastics?". Science of the Total Environment, 755, 142658, 2021.
- [8] Onaç C, Kaya A. "The removal of Cr(VI) through graphene oxide based polymer inclusion membrane". Pamukkale University Journal of Engineering Sciences, 24(7), 1343–1347, 2018.
- [9] Acarer S. "Effect of different solvents, pore-forming agent and solubility parameter differences on the properties of PES ultrafiltration membrane". Sakarya University Journal of Science, 26(6), 1196–1208, 2022.
- [10] Maximous N, Nakhla G, Wan W, Wong K. "Preparation, characterization and performance of Al2O3/PES membrane for wastewater filtration". Journal of Membrane Science, 341(1–2), 67–75, 2009.
- [11] Kayanja O, Hassan MA, Hassanin A, Ohashi H, Khalil ASG. "Effect of phase disparity of MoS2 nanosheets on the performance of PES membranes for dual industrial oil-in-water emulsion separation and dyes adsorption". Process Safety and Environmental Protection, 171, 55–70, 2023.
- [12] Aguilar-Sanchez A, Jalvo B, Mautner A, Nameer S, Pöhler T, Tammelin T, et al. "Waterborne nanocellulose coatings for improving the antifouling and antibacterial properties of polyethersulfone membranes". Journal of Membrane Science, 620, 118842, 2021.
- [13] De Guzman MR, Andra CKA, Ang MBMY, Dizon GVC, Caparanga AR, Huang S-H, et al. "Increased performance and antifouling of mixed-matrix membranes of cellulose acetate with hydrophilic nanoparticles of polydopamine-sulfobetaine methacrylate for oil-water separation". Journal of Membrane Science, 620, 118881, 2021.
- [14] Abdellah Ali SF, William LA, Fadl EA. "Cellulose acetate, cellulose acetate propionate and cellulose acetate butyrate membranes for water desalination applications". Cellulose, 27(16), 9525–9543, 2020.

- [15] Ou R, Wang Y, Zhang H, Wang H, Xu T. "Preparation of high-flux ultrafiltration membranes by blending strongly charged polymer". Journal of Applied Polymer Science, 134(10), 2017.
- [16] Jiang SH, Wu J, Zhou HZ, Jiang CW, Wang J. "The research of hydrophilic modification of PVC/PES blended membrane by the additive of CA". Advanced Materials Research, 1052, 8–13, 2014.
- [17] Liu S, Xu Z, Liu M, Wei Y, Guo F. "Preparation and characterization of PES/CA microporous membranes via reverse thermally induced phase separation process". Polymer Engineering & Science, 58(2), 180–191, 2018.
- [18] Kurniawan TW, Sulistyarti H, Rumhayati B, Sabarudin A. "Cellulose nanocrystals (CNCs) and cellulose nanofibers (CNFs) as adsorbents of heavy metal ions". Journal of Chemistry, 2023, 1–36, 2023.
- [19] Wang X, Chang CH, Jiang J, Liu Q, Liao Y, Lu J, et al. "The crystallinity and aspect ratio of cellulose nanomaterials determine their pro-inflammatory and immune adjuvant effects in vitro and in vivo". Small, 15(42), 2019.
- [20] Daraei P, Ghaemi N, Sadeghi Ghari H. "An ultra-antifouling polyethersulfone membrane embedded with cellulose nanocrystals for improved dye and salt removal from water". Cellulose, 24(2), 915–929, 2017.
- [21] Qu P, Tang H, Gao Y, Zhang L, Wang S. "Polyethersulfone composite membrane blended with cellulose fibrils". BioResources, 5(4), 2323–2336, 2010.
- [22] Bai L, Wu H, Ding J, Ding A, Zhang X, Ren N, et al. "Cellulose nanocrystal-blended polyethersulfone membranes for enhanced removal of natural organic matter and alleviation of membrane fouling". Chemical Engineering Journal, 382, 122919, 2020.
- [23] Boruah P, Gupta R, Katiyar V. "Fabrication of cellulose nanocrystal (CNC) from waste paper for developing antifouling and high-performance polyvinylidene fluoride (PVDF) membrane for water purification". Carbohydrate Polymer Technologies and Applications, 5, 100309, 2023.
- [24] Gharagheizi F. "New procedure to calculate the Hansen solubility parameters of polymers". Journal of Applied Polymer Science, 103(1), 31–36, 2007.
- [25] Huang J, Tang H, Huang X, Feng Z, Su P, Li W. "Hansen solubility parameters-guided mixed matrix membranes with linker-exchanged metal-organic framework fillers showing enhanced gas separation performance". Journal of Membrane Science, 668, 121238, 2023.
- [26] Pang J, Pine AWR, Sulemana A. "Using natural language processing (NLP)-inspired molecular embedding approach to predict Hansen solubility parameters". Digital Discovery, 3(1), 145–154, 2024.
- [27] AlQasas N, Johnson D. "Combined effects of surface roughness, solubility parameters, and hydrophilicity on biofouling of reverse osmosis membranes". Membranes, 14(11), 235, 2024.

- [28] Hansen CM. "Hansen solubility parameters: A user's handbook". Second Edition, Boca Raton: CRC Press Taylor & Francis Group, 2007.
- [29] Meringolo C, Poerio T, Fontananova E, Mastropietro TF, Nicoletta FP, De Filpo G, et al. "Exploiting fluoropolymers immiscibility to tune surface properties and mass transfer in blend membranes for membrane contactor applications". ACS Applied Polymer Materials, 1(3), 326–334, 2019.
- [30] Acarer-Arat S, Tüfekci M, Pir İ, Tüfekci N. "Nanocellulose in polyvinylidene fluoride (PVDF) membranes: Assessing reinforcement impact and modelling techniques". Journal of Environmental Chemical Engineering, 12(6), 114749, 2024.
- [31] Rabbani A, Salehi S. "Dynamic modeling of the formation damage and mud cake deposition using fibration theories coupled with SEM image processing". Journal of Natural Gas Science and Engineering, 42, 157–168, 2017.
- [32] Ezeakacha CP, Rabbani A, Salehi S, Ghalambor A. "Integrated image processing and computational techniques to characterize formation damage". SPE International Conference and Exhibition on Formation Damage Control, Lafayette, Louisiana, USA, 2018.
- [33] Guillen GR, Ramon GZ, Kavehpour HP, Kaner RB, Hoek EMV. "Direct microscopic observation of membrane formation by nonsolvent induced phase separation". Journal of Membrane Science, 431, 212–220, 2013.
- [34] Athira VB, Mohanty S, Nayak SK. "Preparation and characterization of porous polyethersulfone (PES) membranes with improved biocompatibility by blending sulfonated polyethersulfone (SPES) and cellulose acetate (CA) A comparative study". Materials Today Communications, 25, 101544, 2020.
- [35] Batool M, Shafeeq A, Haider B, Ahmad NM. "TiO2 nanoparticle filler-based mixed-matrix PES/CA nanofiltration membranes for enhanced desalination". Membranes, 11, 433, 2021.
- [36] Kusworo TD, Widayat W, Utomo DP. "Fabrication and characterization of nano hybrid cellulose acetatenanoTiO2/crosslinked polyvinyl alcohol coated membrane for crude clove oil purification". Periodica Polytechnica Chemical Engineering, 64(3), 304–319, 2020.
- [37] Drikvand HN, Golgoli M, Zargar M, Ulbricht M, Nejati S, Mansourpanah Y. "Thermo-responsive hydrophilic support for polyamide thin-film composite membranes with competitive nanofiltration performance". Polymers, 14(16), 3376, 2022.
- [38] Gan Q, Wu C, Long L, Peng LE, Yang Z, Guo H, et al. "Does surface roughness necessarily increase the fouling propensity of polyamide reverse osmosis membranes by humic acid?". Environmental Science & Technology, 57(6), 2548–2556, 2023.
- [39] Bildyukevich AV, Plisko TV, Lipnizki F, Pratsenko SA. "Correlation between membrane surface properties, polymer nature and fouling in skim milk ultrafiltration". Colloids and Surfaces A: Physicochemical and Engineering Aspects, 605, 125387, 2020.

- [40] Hobbs C, Taylor J, Hong S. "Effect of surface roughness on fouling of RO and NF membranes during filtration of a high organic surficial groundwater". Journal of Water Supply: Research and Technology-Aqua, 55(7–8), 559–570, 2006.
- [41] Wu Z, Ji X, He Q, Gu H, Zhang W, Deng Z. "Nanocelluloses fine-tuned polyvinylidene fluoride (PVDF) membrane for enhanced separation and antifouling". Carbohydrate Polymers, 323, 121383, 2024.
- [42] Tshabalala TG, Nxumalo EN, Mamba BB, Mhlanga SD. "Synthesis of robust flexible polyethersulfone ultrafiltration membranes supported on non-woven fabrics for separation of NOM from water". Water SA, 42(4), 621, 2016.
- [43] Krishnamoorthy R, Sagadevan V. "Polyethylene glycol and iron oxide nanoparticles blended polyethersulfone ultrafiltration membrane for enhanced performance in dye removal studies". E-Polymers, 15(3), 151–159, 2015.
- [44] Ghasemi H, Abu-Zahra N, Baig U, Waheed A, Aljundi IH. "Surface-engineered polyethersulfone membranes using thermo-responsive poly(N-isopropyl acrylamide) with antibiofouling properties for water treatment applications". Journal of Polymers and the Environment, 32(6), 2589–2605, 2024.
- [45] Nguyen HT, Bui HM. "Bandgap tuning of TiO2 by Cu nanoparticles applied in photocatalytic antifouling-coated PES membranes through PAA-plasma grafted adhesive layer". Water Science & Technology, 87(9), 2390–2405, 2023.
- [46] Selim H, Elshypany R, El-Bahy SM, Mubarak MF, Taha EQ. "Fabrication of electrospun nylon6.12/chitosan @PES

- nanofibrous UF membrane towards dyes rejection from synthetic wastewater". Polymer Bulletin, 80, 977–999, 2023.
- [47] Mohamat R, Bakar SA, Muqoyyanah, Mohamed A, Kamal SNEAM, Othman MHD, et al. "Effect of triple-tail surfactant on the morphological properties of polyethersulfone-based membrane and its antifouling ability". Journal of Materials Science, 57, 16333–16351, 2022.
- [48] Abdel-Naby AS, Al-Ghamdi AA. "Chemical modification of cellulose acetate by diallylamine". International Journal of Current Microbiology and Applied Sciences, 3(6), 10-24, 2014.
- [49] Zhang D, Karkooti A, Liu L, Sadrzadeh M, Thundat T, Liu Y, et al. "Fabrication of antifouling and antibacterial polyethersulfone (PES)/cellulose nanocrystals (CNC) nanocomposite membranes". Journal of Membrane Science, 549, 350–356, 2018.
- [50] Lv J, Zhang G, Zhang H, Zhao C, Yang F. "Improvement of antifouling performances for modified PVDF ultrafiltration membrane with hydrophilic cellulose nanocrystal". Applied Surface Science, 440, 1991–1100, 2018.
- [51] Acarer S. "A review of microplastic removal from water and wastewater by membrane technologies". Water Science & Technology, 88(1), 199–219, 2023.
- [52] Alasiar RH, Kochkodan V, Ahzi S, Barth N, Koç M. "Preparation and characterization of polysulfone membranes reinforced with cellulose nanofibers". Polymers, 14, 3317, 2022.